Volumetric properties of concrete under true tri-axial dynamic compressive loadings

Jian Cui[1], Hong Hao, F.ASCE[2], Yanchao Shi[3], Xihong Zhang[4] and Shi Huan[5]

[1]Ph.D. Student, Tianjin University and Curtin University Joint Research Centre of Structural Monitoring and Protection, School of Civil Engineering, Tianjin University, Tianjin 300072, China. E-mail: jian.cui@tju.edu.cn

[2]John Curtin Distinguished Professor, Tianjin University and Curtin University Joint Research Centre of Structural Monitoring and Protection, School of Civil Engineering, Tianjin University, Tianjin 300072, China (corresponding author). E-mail: hong.hao@curtin.edu.au

[3]Professor, Tianjin University and Curtin University Joint Research Centre of Structural Monitoring and Protection, School of Civil Engineering, Tianjin University, Tianjin 300072, China. E-mail: yanchaoshi@tju.edu.cn

[4]Research Fellow, School of Civil and Mechanical Engineering, Curtin University, Bentley, WA 6102, Australia. E-mail: xihong.zhang@curtin.edu.au

[5]Professor, School of Civil Engineering, Guangzhou University, Guangzhou 510006, China. E-mail: huanshi@gzhu.edu.cn

Abstract: Almost all the available test data of pressure-volumetric strain curve (Equation of State, EoS) of concrete are based on static tri-axial tests and one-dimensional impact tests, e.g. flyer-plate-impact test, owing to the lack of equipment to conduct the synchronized tri-axial impact tests. The EoS based on static tri-axial and dynamic uniaxial tests does not necessarily represent the true behaviors of concrete under hydrodynamic loadings. Therefore, to derive accurate dynamic EoS of concrete material, it is essential to develop reliable techniques for conducting true synchronized tri-axial impact tests. This paper presents an innovative three-dimensional Split-Hopkinson Pressure Bar (SHPB) test system developed by the authors recently, and some preliminary test results. A comparison of the true tri-axial dynamic test results and the true tri-axial static test results are carried out. It is found that the bulk modulus of concrete material is strain rate sensitive. Theoretical and numerical analyses with a mesoscale model are carried out to examine and explain the test observations. It is found that the increase in bulk modulus under hydrodynamic loadings can be, at least partially, attributed to the water-pressure because the pore-water in the cement paste cannot be drained during the dynamic loading phase. The resistance of microscopic viscosity to the development of micro-cracks is another reason for strain rate sensitivity of the bulk modulus. An empirical relation is proposed in this study for the Dynamic Increase Factor (DIF) of the concrete bulk modulus with respect to the strain rate.

Keyword: Concrete dynamic properties; Equation of State; SHPB; true tri-axial test.

1. Introduction

Concrete structures during their service life are exposed to multi-hazard loadings such as the blast and impact loadings. Under the action of such high-rate dynamic loads concrete material experiences complex multi-axial stress states caused by propagation of shock waves and inertial confinements. Therefore, understanding the concrete material behaviors under multi-axial dynamic stress states is essential for accurate analysis and economic design of concrete structures to resist blast and impact loads. It is especially important to understand the behavior of concrete under high hydrostatic/hydrodynamic pressures within the range of hundreds of Mega-pascals and even beyond because a large amount of energy is released within microseconds under high dynamic loadings that makes the concrete material undergo very high pressures (Karinski et al., 2017b). However, the behavior of concrete material under high static pressures is not well studied yet, and the studies of the dynamic volumetric behaviors of concrete under high hydrodynamic pressures are even less owing to the lack of tri-axial dynamic testing facility that can apply synchronized tri-axial dynamic loads. As a result, most existing constitutive models for concrete EoS are compromised with testing data of static tri-axial tests or uniaxial impact tests which may not reliably reflect the true dynamic material properties under tri-axial stress state, and hence lead to inaccurate predictions of concrete structure responses (Cui et al., 2017a).

Numerical simulations have been becoming an important tool in the investigation of the effects of blast and impact on concrete structures. The application of these simulations requires accurate concrete constitutive models. In hydrocodes, the constitutive laws for the volumetric and deviatoric material behaviors are treated separately with an equation of state (EoS) and a strength model (Gebbeken and Ruppert, 2000; Hartmann et al., 2010; Malvar et al., 1997). Generally, experimental studies of EoS of concrete are complex and expensive. For low pressure stage of EoS, the pressure-volumetric strain can be derived through quasi-static tri-axial tests (Burlion et al., 2001; Karinski et al., 2017a; Xiong et al., 2012). For high pressure stage of EoS, dynamic one-dimensional strain tests such as the flyer-plate-impact test are most commonly used (Forquin et al., 2008; Gebbeken et al., 2006; Hall et al., 1999; Riedel et al., 2008). However, obviously static tri-axial tests could not obtain the dynamic properties of concrete, and the dynamic one-dimensional strain tests could not reflect the real behavior of concrete under tri-axial dynamic loads (Cui et al., 2017a). EoS derived from such tests therefore does not necessarily reflect the true behavior of concrete material under high hydrodynamic pressures. Since EoS influences not only the wave propagation in solids, but also the strength and damage of concrete because the current pressure in the principal stress space is determined from the EoS in the explicit time integration algorithm (Malvar and Simons, 1996), it is therefore essential to derive the EoS that truly reflects the concrete material behavior under hydrodynamic loads. Ideally, this can be done by performing true tri-axial dynamic tests.

Owing to the inherent difficulty in performing hydrodynamic tests because of the challenge in applying synchronized tri-axial dynamic loads, some researchers conducted pseudo tri-axial dynamic tests, i.e., uniaxial impact tests on specimens with a predefined lateral confinement pressure or using the steel wrap to provide lateral confinement on specimens. The test results are used to derive the dynamic material properties under multi-axial stress states. Such tests give more realistic dynamic material properties under multi-axial stress states than those based on uniaxial impact tests without applying any lateral confinements. However, as proved by the authors in a previous study that it is very difficult to obtain accurate multi-axial dynamic material properties with the current test apparatus because the confinement pressure varies with the specimen deformation and is not controllable (Cui et al., 2017b). Therefore, it is important to develop reliable techniques to conduct true synchronized tri-axial impact tests. In this paper, an innovative design of three-dimensional SHPB device for dynamic tri-axial tests is presented. It can generate equal-amplitude and synchronized dynamic impact loadings in the three principal directions on the testing specimen. Therefore, it can be used to study the EoS of concrete under tri-axial dynamic loadings. Some preliminary testing results are presented. The corresponding static tri-axial tests with the same concrete specimens were also carried out and the results are compared and discussed (Cui et al., 2017c). To better examine and explain the observed strain rate effects on EoS, theoretical and numerical analyses are also conducted. It is found that the existing pore water in the concrete specimen contributes to the increase in the bulk modulus of concrete material with strain rate under hydrodynamic loads. An empirical relation is proposed in this study to model the bulk modulus enhancement of concrete under high dynamic loadings.

2. Volumetric properties of concrete under static tri-axial loadings

2.1 Concrete specimens

The unconfined uniaxial strength of specimen was designed to be 30 MPa and the mix properties are given in **Table 1**. Natural river sand was used as the fine aggregate and cleaned gravels with a maximum size of 10 mm were used as the course aggregate. The specimens were cast in a 50 mm cubic metal mold. After removal from the mold, they were cured in a standard moist chamber with relative humidity of more than 90% and temperature of around 20℃ for 28 days. The average uniaxial compressive strength of the four specimens were tested to 35.2 MPa at the beginning of the test process.

Table1 Mix proportions of the studied concrete

Cement (kg/m^3)	339
Cement Type	Portland 42.5R
Water(kg/m^3)	231
Coarse Aggregate (kg/m^3)	1041
Fin Aggregate (kg/m^3)	789

2.2 Equipment

The experiments were conducted by a true tri-axial hydraulic servo-controlled test system in Central South University in China (Li et al., 2015). This apparatus applies quasi-static loads along the three principal directions (X, Y and Z axes) through hydraulically driven pistons independently. High-strength steel (20CrNiMo), which has a yield strength of 785 MPa and an elastic modulus of 210 GPa, is used to transfer the applied loads from the actuators to the specimen as shown in **Fig. 1**. The side length of the steel load transfer bar is 47 mm, 3 mm shorter than the side length of the cubic specimen (50 mm) to avoid collision of the load transfer bars in different directions when the specimen experiences a large strain during the loading process, as illustrated in **Fig. 1**. The axial loads are recorded by the load cells, and the deformation of the specimen is measured by LVDT sensors. The elastic deformation of the load transfer bar is removed from the measured deformation in the subsequent data analyses to obtain the strain of the tested specimen. More detailed descriptions of the test facility can be found in (Cui et al., 2017c).

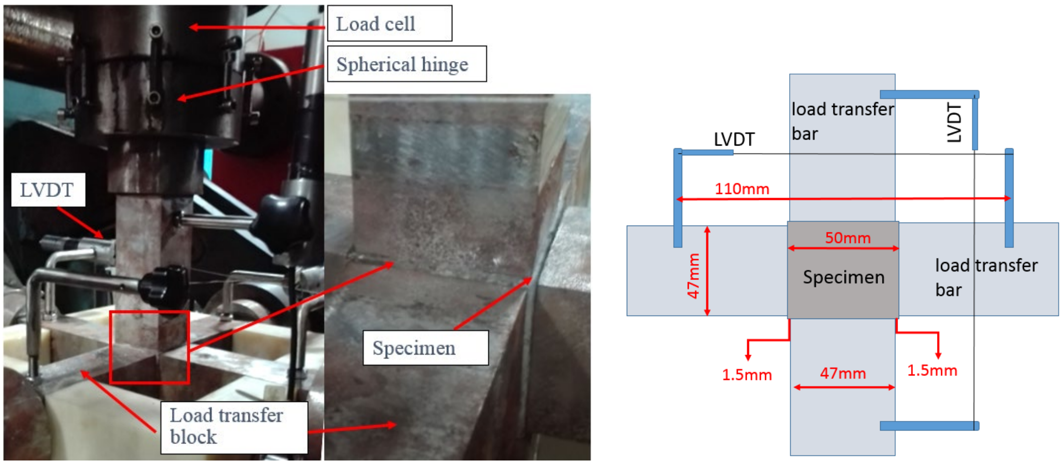

(a) (b)

Fig. 1 The test set-up: (a) overall view; (b) 2D section view

2.3 Test results

The specimen is kept in a hydrostatic stress state to study the volumetric properties of concrete. To ensure $\sigma_1 = \sigma_2 = \sigma_3$ (σ_1, σ_2, and σ_3 are the three principal stresses, respectively) during the loading-unloading process, the forces of X, Y and Z axes are applied by the force control mode at a rate of 1 kN/s (0.4 MPa/s) until reaching 500 MPa. More details of the test procedures and loading protocols can be found in (Cui et al., 2017c).

Fig. 2 gives a typical hydrostatic pressure-volumetric strain curve of the tested concrete specimen. It should be noted that our specimens were tested and the results of which are very close. The pressure p is the mean value of the three principal stresses, which are almost identical. The volumetric strain can be obtained by summing the three principal strains, i.e., the strain of the X, Y and Z directions. It can be seen that at the beginning of the loading process, the pressure-volumetric curve is almost a straight line which indicates that the concrete is in an elastic stage. It starts to have a plastic deformation when the pressure reaches about 90% of the uniaxial compressive strength. Then pore crush and cement matrix damage may occur gradually which leads to the reduction of the bulk modulus. Under 500 MPa pressure, the volumetric strain of the specimen is about 11%.

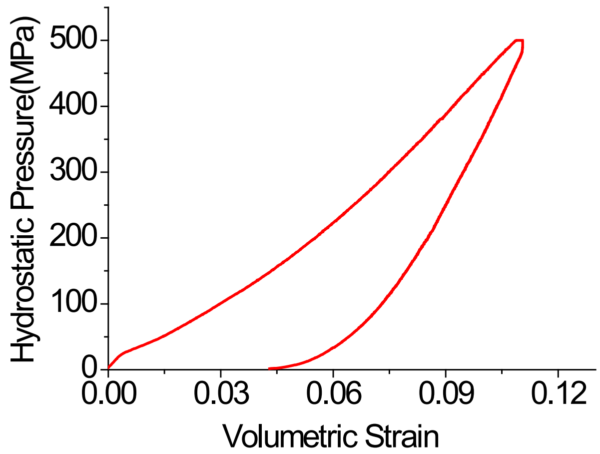

Fig. 2 Hydrostatic pressure-volumetric strain curve

3. Volumetric properties of concrete under tri-axial impact loadings

In this section, a three-dimensional SHPB (3D-SHPB) test system developed recently by the authors is briefly introduced. The test system is made to perform synchronized tri-axial dynamic loading tests, hence to derive the testing data for development of dynamic EoS of materials. Some preliminary tests on the same 50 mm concrete specimens have been conducted using the system. The static and dynamic tri-axial testing data are compared to directly investigate the strain rate effects on EoS of concrete material.

3.1 Three - dimensional SHPB test system

The schematic illustration of the 3D-SHPB system is shown in **Fig. 3** and the photo of the device is shown in **Fig. 4**. The device consists of three cylindrical incident bars and three cylindrical transmitted bars of 50 mm in diameter. As shown in **Fig. 4**, the incident bars are vertically installed on the platform, which are above the ground. The pressure vessel is at the bottom of the apparatus. A striker bar with 120 mm in diameter impacts the three incident bars (50 mm in diameter) simultaneously to induce synchronized stress waves in the three incident bars, as shown in **Fig. 5**. At the top of the apparatus, three transmitted bars are positioned on the support frame, which stand on the operating platform. Each of the transmitted bars is accurately aligned to guarantee their symmetrical arrangement over the platform with the help of fine adjustment screws on the support frame. As shown in **Fig. 4**, three incident transformation heads (ITH) are attached to the upper end of three incident bars respectively, and three transmitted transformation heads (TTH) to the lower end of transmitted bars. The three ITHs were carefully designed and manufactured. They change the contact surface from circular (incident bar) to square (specimen), as well as the wave direction, i.e., from the vertical direction to three perpendicular directions to generate synchronized tri-axial impact on a cubic specimen. As will be demonstrated later the design successfully generated synchronized tri-axial impacts on specimens. On the other sides of the specimen, the three TTHs are used to change the contact surface from square back to circular for connecting to the three transmitter bars. Strain gauges are glued on the three incident bars and the three transmitter bars to record the strain and to derive the stress time histories, similarly to that in a traditional 1D-SHPB test.

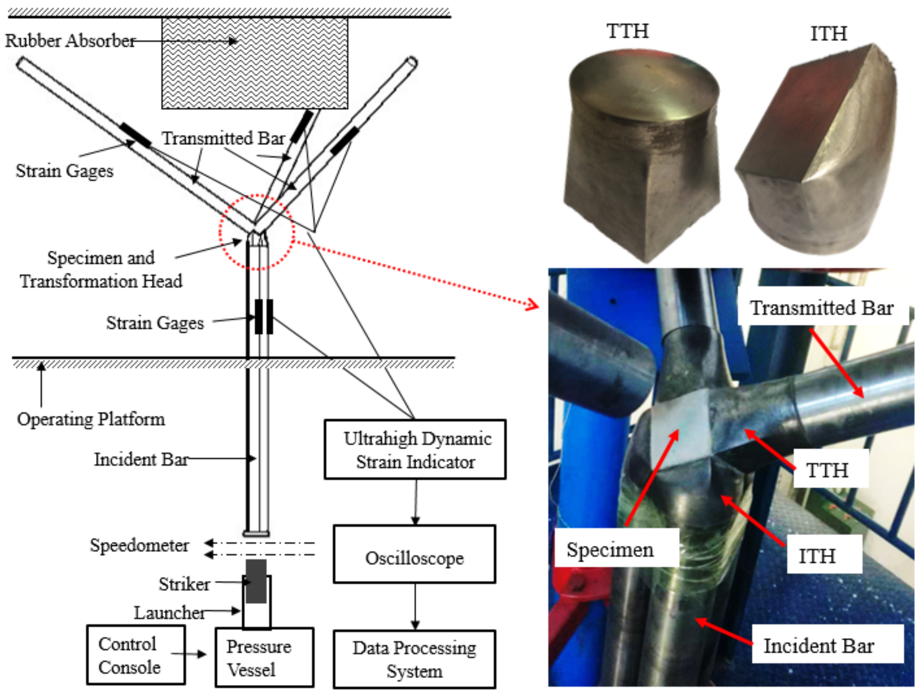

Fig. 3 Schematic illustration of the three-dimensional SHPB system

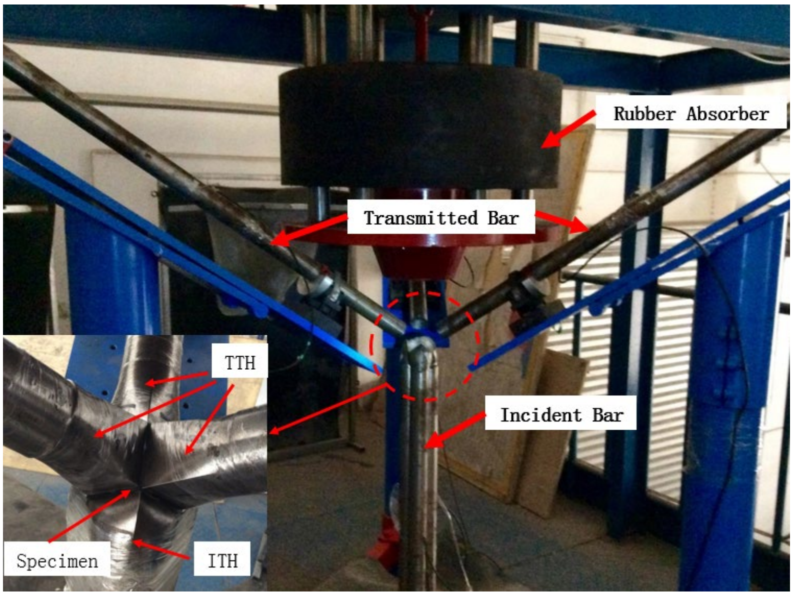

Fig. 4 Photograph of the three-dimensional SHPB system

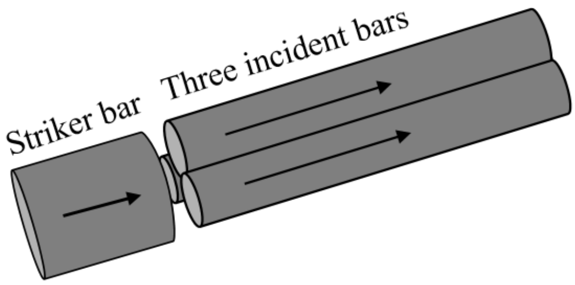

Fig. 5 Schematic illustration of the strike bar and incident bars

3.2 Verification of the test system

The primary concerns of the device are its ability to 1) generate synchronized tri-axial impact; and 2) generate only axial impact without or with only minimum shear stress waves on the specimen from the ITH. Only these two conditions are satisfied, the device can be considered to be able to performing true tri-axial impact tests. **Fig. 6** shows the typical stresses recorded from a shot of experiment. It can be found that the three incident waves and the three transmitted waves are well synchronized, respectively. Small variations in the amplitudes of the three incident waves could be attributed to the difference between strain gages and operation errors of the tester, and so were the three transmitted waves. However, the difference is relatively small, i.e., less than 8%. The measured transmitted waves indicate the designed 3D-SHPB system can generate synchronized and equal-amplitude impact stresses on the cubic specimen.

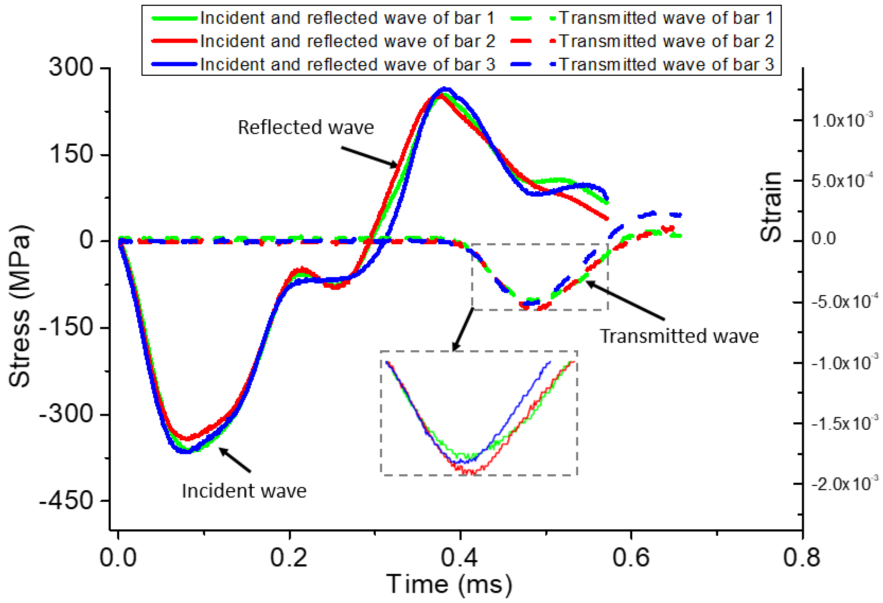

Fig. 6 Stress histories in the bars during the impact test

Another concern of this design is the change of the wave direction by using ITH, which might result in significant shear waves, therefore complicates the stress state in the specimen and makes the loading condition not purely tri-axial impacts. Ideally, the specimen should be only subjected to equal-amplitude and synchronized axial impact loadings in the three principal directions. To check if the ITH only transmits the axial wave primarily, two strain gauges were placed on the opposite surface of a transmitted bar, as shown in **Fig. 7**. Before the test, the contact surfaces between ITH and the specimen were smoothed by a polisher carefully and coated with grease to reduce the friction force between the specimen and the ITHs which may lead to the shear wave propagating into the specimen and the transmitted bars. The measured stress histories in a transmitted bar are shown in **Fig. 8**. As shown in the figure, the signals recorded by the two strain gauges on the opposite sides of the bar are almost the same, and the maximum difference is less than 5%. This indicates that the shear wave in the transmitted bar is small and can be neglected. These observations demonstrate the success of the designed ITH in transmitting the axial wave and minimizing the shear wave.

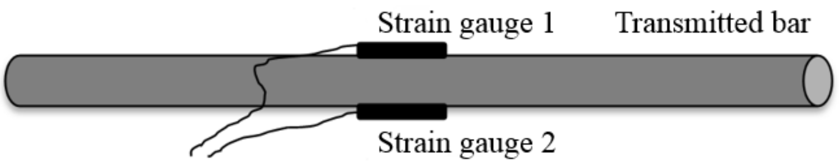

Fig. 7 Positions of the two strain gauges on the opposite surfaces of the transmitted bar for verifying the shear wave effect

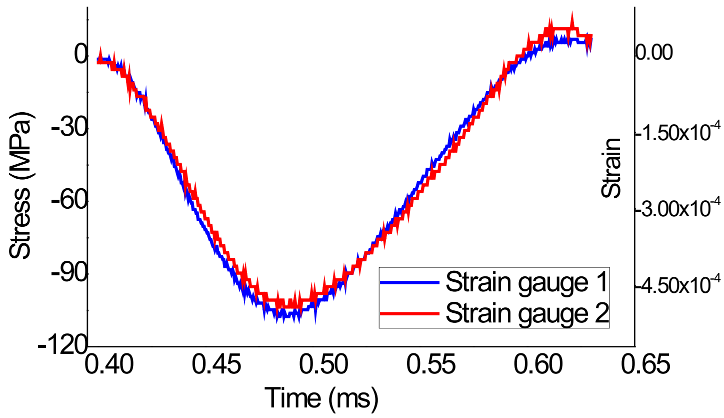

Fig. 8. The stress histories recorded by the two strain gauges on the opposite surfaces of the transmitted bar

3.3 Test results

The compression stress in the specimen can be deduced from the axial strain signals of strain gauges on the elastic transmitted bars. The compression stress of the specimen is (Xiao et al, 2015):

$$\sigma = \frac{A_t E \varepsilon_t}{A_s} \tag{1}$$

where A_t and A_s are cross sectional area of the transmitted bar and the specimen, respectively; E is the Young's modules of the steel bar and ε_t is the axial strain of the transmitted bar measured by strain gauges. As shown in **Fig. 6** the transmitted waves from the three principal directions are almost the same. Therefore, the dynamic pressure p is taken as the mean value of the three principal stresses.

The schematic illustration of strain analysis for specimen is provide in **Fig. 9**. The particle velocity at the end of ITH and TTH are v_1 and v_2, respectively. Thus the strain rate of the specimen is

$$\dot{\varepsilon} = \frac{v_1 - v_2}{l} \tag{2}$$

where l is the length of the specimen.

$$v_2 = C_B \cdot \varepsilon_t \tag{3}$$

$$v_1 = C_B \cdot (\varepsilon_{in} - \varepsilon_r) \tag{4}$$

$$\varepsilon_{in} = \varepsilon_i \cdot \cos\theta \tag{5}$$

where C_B is the velocity of stress wave in the steel bar, ε_i, ε_t and ε_r represent the incident strain, transmitted strain and reflected strain from the strain gauges on the bars. ε_{in} is the axial component of the incident strain along the longitude direction of the transmitted bar, as shown in **Fig. 9**. ε_i, ε_t can be measured by the strain gauges on the incident bars and transmitted bars. However, the reflected strain cannot always be reliably measured by the strain gauges on the incident bar like one-dimensional SHPB test system because its propagating direction is not along the axis of the incident bar.

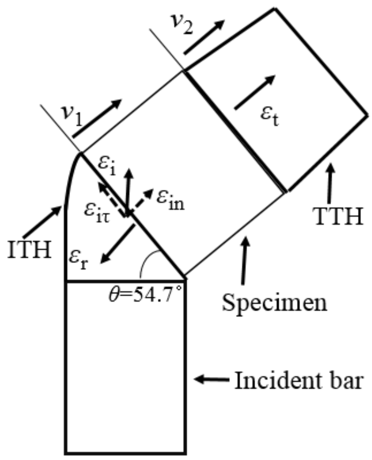

Fig. 9 Schematic of the strain analysis for the specimen

To analyze the SHPB test results, the following two postulates must be satisfied: (1) the stress wave in the bar is one-dimensional elastic wave; (2) stress and strain states within the specimen are uniform. For the first postulate, the requirement of elastic deformation in the pressure bar can be satisfied by limiting the impact velocity. The stress wave can also be regarded as one-dimensional if the diameter of the bar is much smaller than the length of the wave and the input wave is along the axial direction of the bar. These issues are considered well at the time of design of the device. The influence of transverse component of the incident strain $\varepsilon_{i\tau}$ has been studied above (**Fig. 8**) that there are almost no shear waves being transmitted into the specimen and the transmitted bars. However, one-dimensional postulate is violated for the reflected wave because the reflected wave is not along the axial direction of the incident bar. In other words, the recorded reflected waves shown in **Fig. 6** cannot be directly used. It means that only the incident waves and the transmitted waves can be used to analyze the test results. Therefore, the standard approach in uniaxial SHPB test cannot be directly adopted here, i.e., the reflected wave which reflects the strain and the strain rate of the specimen only can be calculated by the incident wave and the transmitted wave under the premise of the second postulate of stress equilibrium. For the second postulate, it is influenced by the material properties and the slenderness (l/d) of the specimen. For concrete material, specimens with the slenderness around 1.0 has been used in many studies (Li and Meng, 2003; Lv et al., 2017; Meng and Li, 2003). According to the study of Yang and Shim (Yang and Shim, 2005), it needs 3 – 4 times of wave transits for reaching stress uniformity of concrete material under an input pulse with a finite rise time. In this study, the loading time is about 0.1 ms as shown in **Fig. 6** and the sound velocity of the 50 mm cubic specimen is about 4000 mm/ms (Cui et al., 2017c) , hence the number of wave transit from one end of the specimen to the other can reach 8 times during the loading time. Therefore, the postulate of stress equilibrium can be considered true in this study.

Then the reflected strain ε_r can be derived according to the equation of stress equilibrium

$$\varepsilon_r = \varepsilon_t - \varepsilon_{in} = \varepsilon_t - \varepsilon_i \cdot \cos\theta \tag{6}$$

Therefore, the strain of specimen is

$$\varepsilon = -2\frac{C_B}{l}\int_0^t \varepsilon_r dt \tag{7}$$

Then the dynamic volumetric strain ε_v can be obtained by summing the strains of the specimen in the three perpendicular directions. As the three incident waves and the three transmitted waves are the same, the three principal strains of specimen get from Eqs (6)-(7) are also the same ($\varepsilon_1 = \varepsilon_2 = \varepsilon_3 = \varepsilon$, $\varepsilon_v = 3\varepsilon$).

Fig. 10 shows the EoS derived from the 3D SHPB tests and the static tri-axial tests using the same concrete specimens. It can be seen from the figure that the bulk modulus of the concrete from the dynamic test is higher than that from the static test. On the other hand, it can be seen that at low pressure, the slopes of the tangent lines (the thin lines) differ a lot, i.e., the one under the dynamic loading is higher than that under the static loading, while at high pressure, they tend to converge. This means that the strain rate sensitivity on modulus decreases with the increment of the pressure. This is because the pore-structure of concrete will be thoroughly destroyed when the concrete is fully compacted. Therefore, the effect of free water in the pores which contributes to the strain rate sensitivity of bulk modulus (detailed in the section 4) will disappear. The EoS derived from the dynamic tests also includes an elastic stage and a plastic pore crush stage although the transition point between the two stages is not as distinct as that in the static test result. The initial compaction stress P_e also increases with the increment of strain rate.

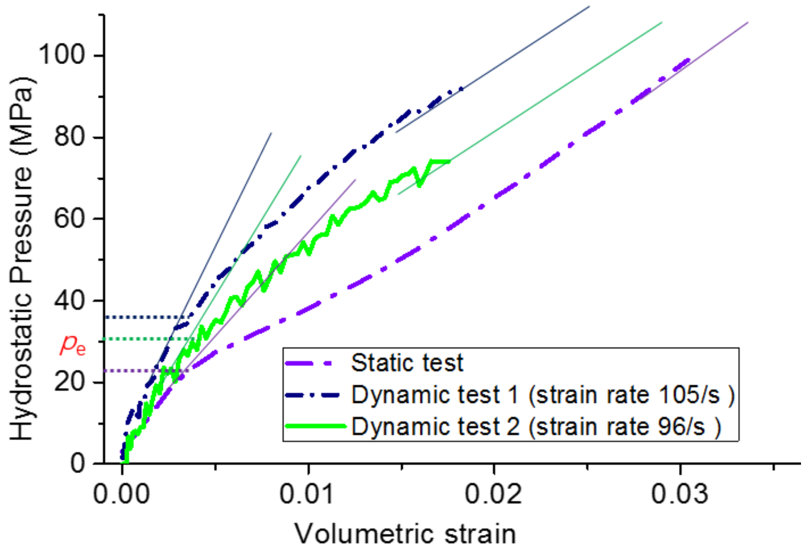

Fig. 10 EoS from the static test and dynamic tests

The presented results have gone through rigorous examination and validation process, i.e. repeatability of the incident and transmitted wave signals, alignment of the incident wave arrival time and magnitudes, and dynamic equilibriums in each direction. It is challenging for carrying out tri-axial dynamic testing of concrete materials. The successful rate of obtaining good testing data with the current design is only about 20%, which makes the tests very time consuming and expensive. On the other hand, some parts of the device such as ITHs and TTHs could be damaged under very high rate loadings owing to their colliding with each other. Changing the parts of the device is expensive. Currently modifications to improve the design of the device are underway. Therefore, only some typical testing data are presented here to demonstrate the device and to show the material behavior of concrete under synchronized tri-axial impact at different strain rates.

It should be noted that the limited testing data obtained so far are the first ever in literature for concrete material under synchronized tri-axial impact loads. It demonstrates for the first time the strain rate sensitivity of concrete material under hydrodynamic loads.

4. Explanation of strain rate effect on bulk modulus of concrete material

Testing data in **Fig. 10** indicates the bulk modulus of concrete material is strain rate dependent, and increases with the strain rate. Previous studies revealed that concrete material properties are less strain rate sensitive under confinement because the confining pressure constrains the development of large cracks hence resulting in widely distributed cracks in the specimen with many small fragments, similar to the failure mode of the specimen under high-speed impact (Cui et al., 2017b). Therefore, it makes the material less strain rate sensitive. The observed strain rate effect on EoS of concrete material under synchronized tri-axial impact is believed being caused by pore water pressure in the concrete specimen. The pore structure of concrete is one of its most important characteristics and influences its mechanical behavior. Various contents of free water distribute in the pores depending on the ambient humidity. This section explains the strain rate effect of bulk modulus under hydrodynamic loadings caused by water-pressure and water viscosity.

4.1 Influence of water-pressure

4.1.1 Theoretical explanation of water-pressure effect

The increment of bulk modulus under high loading rates may be attributed to the existing water in the mortar. As shown in **Fig. 11**, in the schematic microstructure of the mortar, some pores are fully filled with water and some are not. These pores are connected by the capillaries. Under hydrostatic loadings, the compaction makes the water flow from the filled pores to the empty or not fully filled ones through capillaries and no water-pressures inside the pore are produced to resist the compaction of the pore. However, under hydrodynamic loadings, the compaction is so fast that the capillaries cannot drain the water timely. Therefore, compaction of the water produces circumferential stresses, which act on the inner-wall of the pore to resist its compaction (**Fig. 11**). This water-pressure in mortar under hydrodynamic loadings makes the pores more difficult to be compacted than that under hydrostatic loadings. Macroscopically, the bulk modulus of concrete increases.

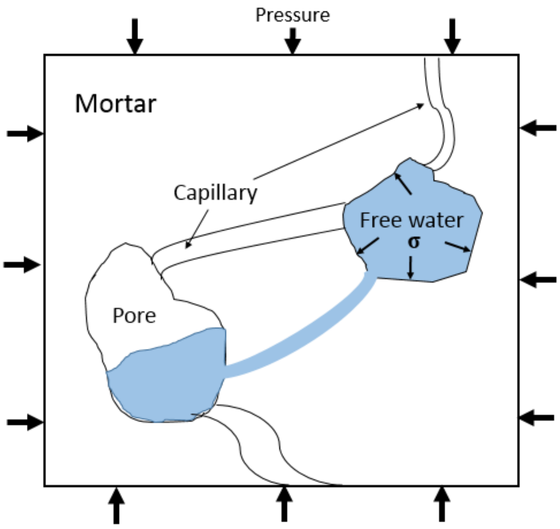

Fig. 11 Water-pressures inside the pore caused by compaction of the free water

To confirm this hypothesis, Tezaghi theory can be used to compute the drainage time approximately. According to the study in (Forquin et al., 2010; Holtz and Kovacs, 1981), if one considers a porous saturated concrete subjected to an oedometric loading and assuming the perfect tightness boundary condition on the lateral surface and a perfect drainage boundary condition on the end faces of the specimen, an analytical solution of drainage time can be derived as

$$t_{\text{drainage}} = \frac{\gamma_{\text{w}} T_{\text{v}} H^2}{4kE_{\text{oedometric}}} \tag{8}$$

where H is the height of specimens (H = 50 mm), k is the permeability coefficient of Darcy Law (k = 11.5e-13 m/s (Forquin et al., 2010; Skoczylas et al., 2007)), $E_{oedometric}$ corresponds to the apparent elastic modulus of concrete from the oedometric test (about 7 GPa), γ_w is the volume-weight of water (γ_w = 9810 N/m^3) and T_v is an adimensional time (T_v equals 0.2 for a drainage of 50%). Therefore, the time corresponding to 50% of drainage for the concrete specimen is computed to be 152 s. Certainly, in this study the concrete is not in the above ideal conditions, i.e., the concrete is not completely saturated, and it is subjected to a tri-axial loading and all the surfaces of the specimen are drainage boundary (not only the end faces). However, during the dynamic loading time of 0.1 ms (comparing to 152 s needed for 50% of drainage), it is reasonable to assume almost no water can be drained during the impact.

Some work of Forquin et al.(Forquin et al., 2010) can also verify the above assumption. Forquin et al. carried out the confined compression tests of concrete specimens using a modified one-dimensional SHPB device. As shown in the **Fig. 12** (a), for dynamic tests (V8.5 DRY means the velocity of striker bar is 8.5 m/s, the specimen is dry), the bulk modulus of wet concrete is higher than the dry concrete. On the other hand, as shown in the **Fig. 12** (b), The result of testing case QS WET-55s (quasi-static test of a wet specimen with a loading time of 55 seconds) is close to that of the dynamic test case V11 WET because 55 seconds are not enough for drainage. However, when the loading rate is very low, the result of the quasi-static test of the wet specimen (QS WET-24H) is similar to that of the dry one (QS DRY-20min) because 24 hours are enough for all the water to be drained so that there is no resistance from pore water.

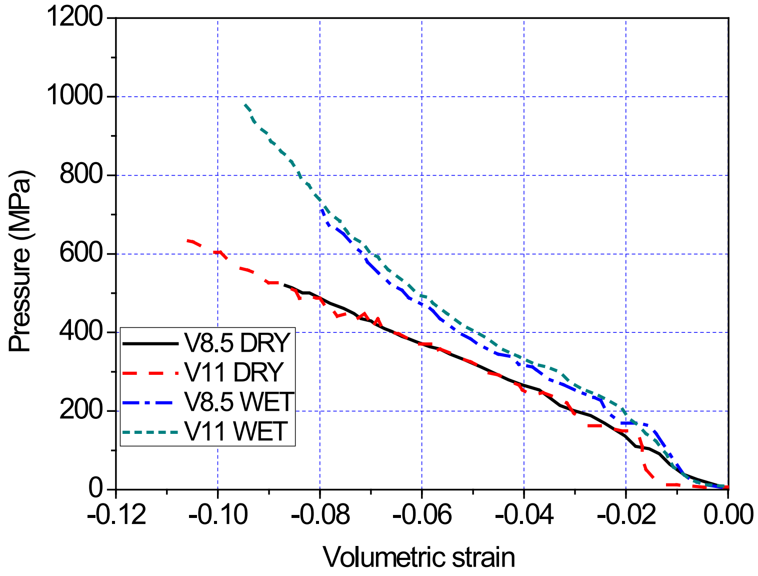

(a)

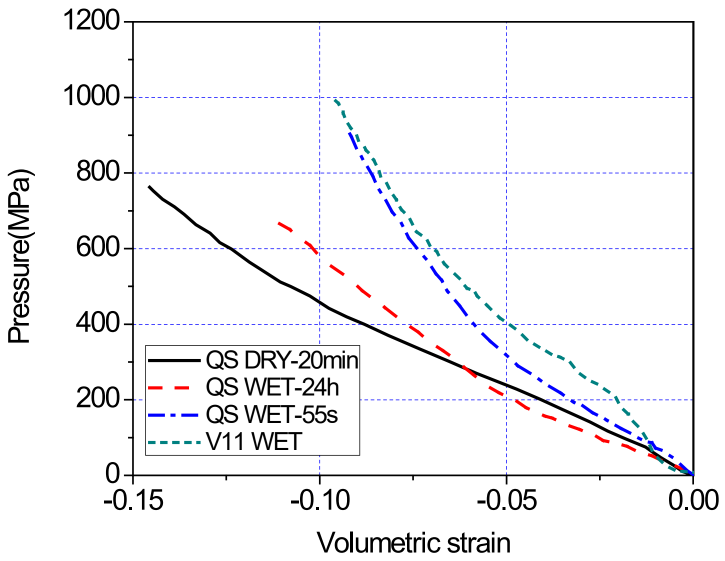

(b)

Fig. 12 Pressure - Volumetric strain curves of different concrete specimens under different loadings(Forquin et al., 2010)

4.1.2 Numerical study of water-pressure effect

To better understand the influence of free water on concrete properties, a mesoscale numerical model with randomly distributed pores is established. It should be noted that the microstructure of concrete is extremely complicate, the pores that can store free water vary from about 0.5 nm to about 50 um (Kumar and Bhattacharjee, 2003) which makes numerically model a realistic concrete specimen with randomly distributed pores nearly impossible with the current computer power. The shapes of the micro-pores also vary a lot. This simulation is performed to explain the influence of water-pressure on bulk modulus rather than to quantify it. Therefore, only a simplified model is built. A FORTRAN program is developed to generate randomly distributed pores in the finite element meshes of the cement paste. The specimen size is 10 mm cubic and the total volume of pores is assumed to be 5%. A Lagrange solid elements of 0.2 mm is used for modelling cement paste and pore-water. The pore size is also assumed to be 0.2 mm. Details of the development of this kind of model are provided in references (Chen et al., 2015; Cui et al., 2018). For brevity they are not repeated here.

K&C model (Malvar et al., 1997) in LS-DYNA (R7.0.0) is used to model the mortar in the simulation. The EoS employed in LS-DYNA by the K&C model is defined using tabular input to define the relationships between volumetric strain and pressure. The automatic parameter generation for K&C model is used in the simulation and the input material parameters are listed in Table 2.

Table 2 Material parameters of mortar

Parameters	Density (kg/m^3)	Poisson's ratio	Strength (MPa)
value	2100	0.19	35

Null material and GRUNESIEN Equation of State in LS-DYNA are used to simulate water pressure.

In compression, the pressure is given by,

$$p = \frac{\rho_0 C^2 \mu \left[1 + (1 - \frac{\gamma_0}{2})\mu - \frac{a}{2}\mu^2\right]}{\left[1 - (S_1 - 1)\mu - S_2 \frac{\mu^2}{\mu+1} - S_3 \frac{\mu^3}{(\mu+1)^2}\right]^2} + (\gamma_0 + a\mu)E \tag{9}$$

where ρ_0 is the initial density of fluid; $\mu = \rho/\rho_0 - 1$, and ρ is the density after disturbance; C is the sound speed; γ_0 is the Gruneisen coefficient, and a is the volume correction coefficient; S_1, S_2 and S_3 are fitting coefficients; E is the specific internal energy per unit volume, the initial applied pressure is controlled by the input value of initial internal energy. These parameters are given in Table 3 (Liu et al., 2002).

Table 3. Material parameters and coefficients in the EoS for water (Liu et al., 2002)

Symbol	ρ_0 (kg/m^3)	C (m/s)	γ_0	a	S_1	S_2	S_3
Value	1000	1480	0.5	0	2.56	1.99	1.23

The numerical models are shown in **Fig. 13**. In model 1, the pores are filled with water and the water cannot be drained. This case is to simulate that the water cannot be drained timely (derived from the Eq. (8)) and the water-pressure is generated under the hydrodynamic tests. In model 2, the pores are empty to represent that the water can be drained, i.e., no water-pressure is generated. Compressive stresses are applied on the three orthogonal surfaces of the specimen with displacement control at a rate of 0.01m/s. The normal directions of the other surfaces are constrained in the numerical model. This gives the average strain rate of 1.0 1/s, i.e 0.01m/s divided by the specimen dimension of 10 mm.

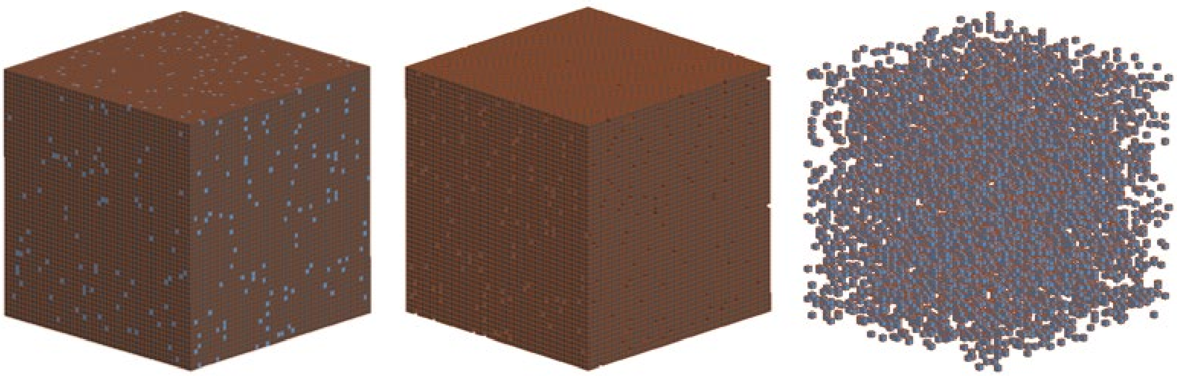

(a) Model 1 (b) Model 2 (c) water

Fig. 13 Cement paste model with randomly distributed pores: (a) Cement paste filled with water (model 1); (b) Cement paste with empty pores (model 2); (c) Water

The simulation results shown in **Fig. 14** demonstrate that the compaction of the free water in the pores can increase the bulk modulus of the cement paste obviously. This explains the bulk modulus of concrete increases under the hydrodynamic loadings caused by undrained pore-water clearly.

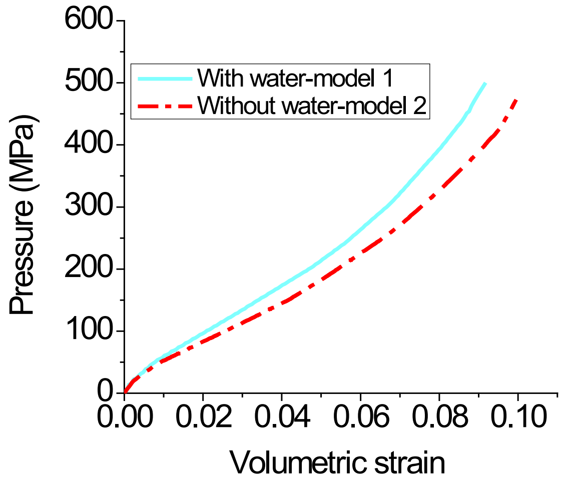

Fig. 14 Influence of water-pressure on bulk modulus of concrete

4.2 Influence of water viscosity

In the second stage of EoS (**Fig. 2**), the volumetric strain is plastic and the bulk modulus of concrete is lower than that of the first elastic stage. In general, the reduction in bulk modulus in the second stage of EoS is caused by the pore collapse when the applied pressure is beyond the pore crush pressure (Borrvall and Riedel, 2011). However, according to the recent study by the authors, development of cracks around the ITZ (interfacial transition zone) is another reason of reduction in bulk modulus when the applied hydrostatic pressure is high(Cui et al., 2017c). As shown in **Fig. 15**, The generation of the cracks under hydrostatic loadings is obvious because concrete is not a homogeneous and isotropic material that even under hydrostatic pressure the stresses inside the concrete specimen are not evenly distributed (Cui et al., 2018).

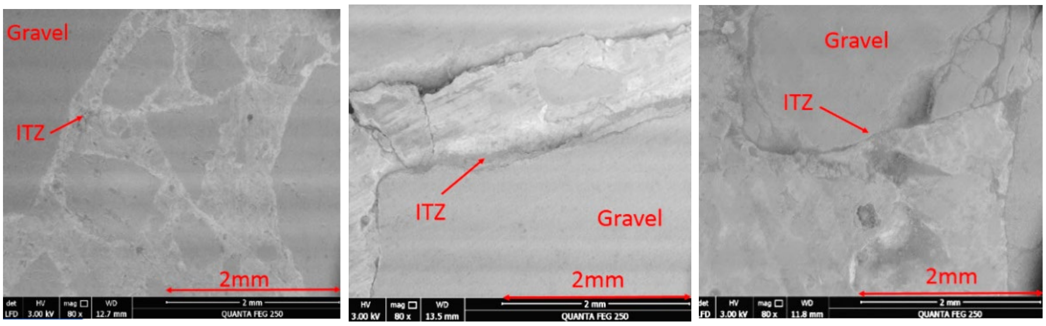

(a) (b) (c)

Fig. 15 Electron microscope photos of concrete: (a) virgin concrete; (b), (c) concrete after application of 500 MPa hydrostatic pressure(Cui et al., 2017c)

Many published works have verified the influence of free water viscosity on the concrete dynamic properties (Fu et al., 2017; Rossi, 1991; Rossi and Toutlemonde, 1996; Rossi et al., 1992). The strength enhancement of concrete under dynamic loadings is attributed to the "Stefan-effect" which leads to the development of microscopic viscous forces within the saturated nanopores (Sercombe et al., 1998; Toutlemonde, 1994) (gel pores, the average width of which is ≤ 3 nanometres) that resist the slip of the micro-cracks (**Fig. 16**).

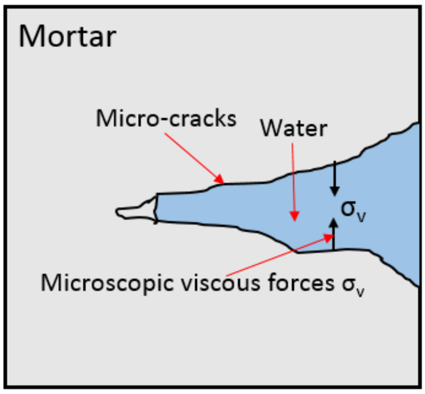

Fig. 16 Microscopic viscous force in mortar at high loading rates

The increase of the bulk modulus under hydrodynamic loadings can also be attributed to the resistance of microscopic viscous force to the development of the micro-cracks, i.e., the viscous forces delay the creation and propagation of the micro-cracks. In other words, the viscous effects in the nanopores harden the cement paste.

5 Consideration of strain rate effect on bulk modulus

Because of the lack of testing data, almost all the current concrete EoS model assume concrete bulk modulus is strain rate independent. This assumption is not accurate as demonstrated and discussed above. Based on the limited testing data of this study, suggestions on modifications of the current concrete EoS models by taking the strain rate effect into consideration are discussed here. For low pressure stage of EoS in the concrete constitutive model, most of the test data are derived from static tri-axial tests (Burlion et al., 2001; Karinski et al., 2017a; Xiong et al., 2012). From the above 3D-SHPB test results, it can be seen that the bulk modulus is strain rate sensitive and this sensitivity seems decrease with the increment of the pressure. Therefore, the influence of strain rate on EoS can be represented as:

$$
\begin{gathered}
p = f(\varepsilon_{\mathrm{v}}) \xrightarrow{\text{strain rate}} p = (\mathrm{DIF_r})^a f(\varepsilon_{\mathrm{v}}) \\
a = \begin{cases} 1 & 0 \le \varepsilon_{\mathrm{v}} < \varepsilon_{\mathrm{vr}} \\ (\varepsilon_{\mathrm{vc}} - \varepsilon_{\mathrm{v}}) / (\varepsilon_{\mathrm{vc}} - \varepsilon_{\mathrm{vr}}) & \varepsilon_{\mathrm{vr}} \le \varepsilon_{\mathrm{v}} < \varepsilon_{\mathrm{vc}} \\ 0 & \varepsilon_{\mathrm{v}} \ge \varepsilon_{\mathrm{vc}} \end{cases}
\end{gathered}
\tag{10}
$$

where ε_{v} is the current volumetric strain of concrete during loading process; $\mathrm{DIF_r}$ is the referential dynamic increase factor, which is defined as the ratio of the bulk modulus from the dynamic test results to the static test results at the same referential volumetric strain $\varepsilon_{\mathrm{vr}}$ (For example, from **Fig. 10**, the $\mathrm{DIF_r}$ can take a value of 1.5 at a referential volumetric strain $\varepsilon_{\mathrm{vr}}$ = 0.01 under a strain rate of 100 1/s); a is a reduction factor for increasing pressure; $\varepsilon_{\mathrm{vc}}$ is the compacted volumetric strain, after which the EoS is no longer strain rate sensitive..

The above only gives a frame for defining the strain rate effect on EoS of concrete. Because the available test results are still limited, no material constant is provided yet. More tests are deemed necessary for better determining the value of these parameters. This will be done after the improved 3D-SHPB device is ready.

6. Conclusions

A newly developed 3D-SHPB device which can achieve loading the specimen synchronically in the three mutually perpendicular directions with equal amplitude is introduced in this study. Volumetric properties of concrete under dynamic true tri-axial stress states are studied and find that the bulk modulus of the concrete from the dynamic tests is higher than that from the static tests. However, the strain rate sensitivity seems to decrease as the increment of the pressure. The test results show that the initial compaction stress P_e is also strain rate sensitive. The increase of the bulk modulus under hydrodynamic loadings can be attributed to the following two reasons: (1) compaction of the pore-water generates the water-pressure which makes the pores more difficult to be compacted; (2) microscopic viscous forces delay the creation and propagation of the micro-cracks.

7. Acknowledgments

The authors gratefully acknowledge the support from the National Basic Research Program of China (973 Program) [grant number 2015CB058003], National Nature Science Foundation of China [grant number 51522808] and Australian Research Council [grant number DP160104557] for carrying out this research.

8. References

Borrvall, T., and Riedel, W. "The RHT concrete model in LS-DYNA." *Proc., Proceedings of the 8th European LS-DYNA Users Conference, Strasbourg*.

Burlion, N., Pijaudier - Cabot, G., and Dahan, N. (2001). "Experimental analysis of compaction of concrete and mortar." *International journal for numerical and analytical methods in geomechanics*, 25(15), 1467-1486.

Chen, G., Hao, Y., and Hao, H. (2015). "3D meso-scale modelling of concrete material in spall tests." *Materials and Structures*, 48(6), 1887.

Cui, J., Hao, H., and Shi, Y. (2017a). "Discussion on the suitability of concrete constitutive models for high-rate response predictions of RC structures." *International Journal of Impact Engineering*, 106, 202-216.

Cui, J., Hao, H., and Shi, Y. (2017b). "Numerical study of the influences of pressure confinement on high-speed impact tests of dynamic material properties of concrete " *Construction and Building Materials*, 171, 839-849.

Cui, J., Hao, H., and Shi, Y. (2018). "Study of concrete damage mechanism under hydrostatic pressure by numerical simulations." *Construction and Building Materials*, 160, 440-449.

Cui, J., Hao, H., Shi, Y., Li, X., and Du, K. (2017c). "Experimental study of concrete damage under high hydrostatic pressure." *Cement and Concrete Research*, 100, 140-152.

Forquin, P., Gary, G., and Gatuingt, F. (2008). "A testing technique for concrete under confinement at high rates of strain." *International Journal of Impact Engineering*, 35(6), 425-446.

Forquin, P., Safa, K., and Gary, G. (2010). "Influence of free water on the quasi-static and dynamic strength of concrete in confined compression tests." *Cement and concrete research*, 40(2), 321-333.

Fu, Q., Xie, Y., Long, G., Niu, D., Song, H., and Liu, X. (2017). "Impact characterization and modelling of cement and asphalt mortar based on SHPB experiments." *International Journal of Impact Engineering*, 106, 44-52.

Gebbeken, N., Greulich, S., and Pietzsch, A. (2006). "Hugoniot properties for concrete determined by full-scale detonation experiments and flyer-plate-impact tests." *International Journal of Impact Engineering*, 32(12), 2017-2031.

Gebbeken, N., and Ruppert, M. (2000). "A new material model for concrete in high-dynamic hydrocode simulations." *Archive of Applied Mechanics*, 70(7), 463-478.

Hall, C., Chhabildas, L., and Reinhart, W. (1999). "Shock Hugoniot and release in concrete with different aggregate sizes from 3 to 23 GPa." *International journal of impact engineering*, 23(1), 341-351.

Hartmann, T., Pietzsch, A., and Gebbeken, N. (2010). "A hydrocode material model for concrete." *International Journal of Protective Structures*, 1(4), 443-468.

Holtz, R. D., and Kovacs, W. D. (1981). *An introduction to geotechnical engineering*.

Karinski, Y., Yankelevsky, D., Zhutovsky, S., and Feldgun, V. (2017). "Uniaxial confined compression tests of cementitious materials." *Construction and Building Materials*, 153, 247-260.

Karinski, Y., Zhutovsky, S., Feldgun, V., and Yankelevsky, D. (2017). "The equation of state of unsaturated cementitious composites–A new multiscale model." *International Journal of Solids and Structures*, 109, 12-21.

Kumar, R., and Bhattacharjee, B. (2003). "Porosity, pore size distribution and in situ strength of concrete." *Cement and concrete research*, 33(1), 155-164.

Li, Q., and Meng, H. (2003). "About the dynamic strength enhancement of concrete-like materials in a split Hopkinson pressure bar test." *International Journal of solids and structures*, 40(2), 343-360.

Li, X., Du, K., and Li, D. (2015). "True triaxial strength and failure modes of cubic rock specimens with unloading the minor principal stress." *Rock Mechanics and Rock Engineering*, 48(6), 2185-2196.

Liu, M., Liu, G., and Lam, K. (2002). "Investigations into water mitigation using a meshless particle method." *Shock waves*, 12(3), 181-195.

Lv, T., Chen, X., and Chen, G. (2017). "Analysis on the waveform features of the split Hopkinson pressure bar tests of plain concrete specimen." *International Journal of Impact Engineering*, 103, 107-123.

Malvar, L. J., Crawford, J. E., Wesevich, J. W., and Simons, D. (1997). "A plasticity concrete material model for DYNA3D." *International Journal of Impact Engineering*, 19(9-10), 847-873.

Malvar, L. J., and Simons, D. "Concrete material modeling in explicit computations." *Proc., Workshop on recent advances in computational structural dynamics and high performance computing*, USAE Waterways Experiment Station, 165-194.

Meng, H., and Li, Q. (2003). "Correlation between the accuracy of a SHPB test and the stress uniformity based on numerical experiments." *International Journal of Impact Engineering*, 28(5), 537-555.

R7.0.0, LS-DYNA971. "Livermore Software Technology Corporation. Livermore, CA."

Riedel, W., Wicklein, M., and Thoma, K. (2008). "Shock properties of conventional and high strength concrete: Experimental and mesomechanical analysis." *International Journal of Impact Engineering*, 35(3), 155-171.

Rossi, P. (1991). "A physical phenomenon which can explain the mechanical behaviour of concrete under high strain rates." *Materials and Structures*, 24(6), 422-424.

Rossi, P., and Toutlemonde, F. (1996). "Effect of loading rate on the tensile behaviour of concrete: description of the physical mechanisms." *Materials and structures*, 29(2), 116-118.

Rossi, P., Van Mier, J., Boulay, C., and Le Maou, F. (1992). "The dynamic behaviour of concrete: influence of free water." *Materials and Structures*, 25(9), 509-514.

Sercombe, J., Ulm, F.-J., and Toutlemonde, F. (1998). "Viscous hardening plasticity for concrete in high-rate dynamics." *Journal of engineering mechanics*, 124(9), 1050-1057.

Skoczylas, F., Burlion, N., and Yurtdas, I. (2007). "About drying effects and poro-mechanical behaviour of mortars." *Cement and Concrete Composites*, 29(5), 383-390.

Toutlemonde, F. (1994). "Shock strength of concrete structures; From material behaviour to structure design." Doctoral Thesis, ENPC, Paris (in French).

Xiao, J., Li, L., Shen, L., Poon, C. (2015) " Compressive behaviour of recycled aggregate concrete under impact loading." *Cement & Concrete Research*, 71, 46-55.

Xiong, Y.-b., Chen, J.-j., HU, Y.-l., and WANG, W.-p. (2012). "Study on the key parameters of the Johnson-Holmquist constitutive model for concrete." *Engineering Mechanics(in Chinese)*, 1, 020.

Yang, L., and Shim, V. (2005). "An analysis of stress uniformity in split Hopkinson bar test specimens." *International Journal of Impact Engineering*, 31(2), 129-150.